Ab initio and photoemission study of correlation effects in $SrRuO_3$ thin films

S. Grebinskij,[1,*] Š. Masys,[2,†] S. Mickevičius,[1,‡] V. Lisauskas,[1,§] and V. Jonauskas[2,|]

[1]*State Scientific Research Institute, Center for Physical Sciences and Technology, A. Goštauto Street 11, LT-01108 Vilnius, Lithuania*

[2]*Institute of Theoretical Physics and Astronomy, Vilnius University, A. Goštauto Street 12, LT-01108 Vilnius, Lithuania*

(Received 27 April 2012; published 4 January 2013)

We present the experimental and theoretical study of correlation effects in epitaxial $SrRuO_3$ thin films. Experimentally, we have performed resonant ultraviolet photoemission spectroscopy (UPS) and angle-resolved hard x-ray photoemission spectroscopy (HAXPES) measurements. For resonant UPS, the two methods, Fano-profile fitting of constant initial state spectra and the energy distribution curves equidistant difference spectra, were used to extract Ru 4*d* partial spectral weight (PSW) in the valence band. We find Ru 4*d* PSW possessing a clearly pronounced coherent peak at the Fermi level together with angle-resolved HAXPES spectra demonstrating no difference in surface and bulk electronic structure. From comparison of experimental data with theoretical calculations done at density functional theory level, we conclude that $SrRuO_3$ is a weakly correlated material and electronic structure of it can be consistently described employing first-principles approaches.

DOI: 10.1103/PhysRevB.87.035106 PACS number(s): 79.60.Dp, 71.20.Be, 71.27.+a

I. INTRODUCTION

$SrRuO_3$ is a ferromagnetic metallic oxide with a partially filled 4*d* shell.[1] Since this perovskite is chemically stable, exhibits excellent electrical conductivity, and has a good lattice matching with various functional oxides, it is the material of choice for electrodes, heterojunctions, and multiferroic devices.[2–7]

One of the most important questions concerning the physics of $SrRuO_3$ is a significance of correlation effects and how physical properties of the material are impacted by correlated movement of electrons.[8] Due to highly extended nature of 4*d* orbitals, it is natural to assume that correlation effects in 4*d* transition metal oxides should be weak. Yet in the literature there are several studies indicating the presence of either weak[9–12] or strong[13–16] electron correlation in $SrRuO_3$. As this issue is of a particular importance, one has to carefully apply experimental and theoretical means while dealing with it.

A powerful experimental tool to investigate the valence states of atoms in solids is resonant photoemission spectroscopy (PES). In Ref. 17, the two methods for evaluation of Ru 4*d* partial spectral weight (PSW) were reviewed. One of them uses photoemission measurements in a photon energy range covering the Ru $4p \rightarrow 4d$ resonance,[14] while the other is based on the Cooper minimum phenomenon of the Ru 4*d* photoionization cross section.[15] However, the experimental measurements for Ru 4*d* PSW presented in Refs. 14 and 15 showed large discrepancies for the main peak intensities in the valence band (VB) region compared to the density functional theory (DFT) results. In their work, Park *et al.*[15] have noticed that band-structure calculations overemphasize spectral weights at the Fermi level. Although the same issue has been addressed in several other works,[13,16,18] considerably sharper peaks in the vicinity of the Fermi level have been recently observed.[19–23] Interestingly, the discrepancy between theoretical and experimental Ru 4*d* spectra is much smaller when thin films of $SrRuO_3$ are grown *in situ*, as in Refs. 19 and 20, or soft x-ray PES is used.[21–24] Since it is well known that PES is highly surface sensitive, the cleaning of *ex situ* prepared specimens by applying heating or scraping techniques may somehow affect the surface and thus further complicate the investigation of intrinsic electronic structure in $SrRuO_3$. Moreover, Siemons *et al.*[19] have concluded that a tiny change in ruthenium stoichiometry may have a fairly considerable effect on the PES spectrum, indicating a highly stoichiometry-dependent degree of correlation for this material. Maiti *et al.*[9] have proposed that the evidence of strong correlation effects in $SrRuO_3$ might be attributed to the change of symmetry at the surface, whereas Rondinelli *et al.*[25] have suggested that electronic behavior of $SrRuO_3$ thin films might be affected by extrinsic factors, such as surface roughness or defects. In addition, one should also take into account the fact that physical properties of this perovskite are sensitive to the strain[26] and thin film thickness.[24]

Having in mind that all these factors may influence the experiment, one should be very careful while making rigorous comments about electronic structure in $SrRuO_3$. It is evident that interpretation of experimental results is highly dependent on accurate theoretical calculations. For this purpose, we have performed theoretical analysis employing the method of linear combination of atom-centered Gaussian orbitals (LCAO). To the best of our knowledge, the LCAO approximation has not yet been applied in the investigation of bulk $SrRuO_3$. Hence, we have a good opportunity to compare our results with recent calculations based on different plane-wave or muffin-tin orbital approaches (see, e.g., Refs. 27–30) and make sure that there are no discrepancies from a theoretical point of view.

Concerning the experiment, we are interested to know whether the improvement of resonant ultraviolet photoemission spectroscopy (UPS) data analysis may help to reduce the reported mismatch between measurements and theory. What is more, the employment of angle-resolved hard x-ray photoemission spectroscopy (HAXPES) allows us to present surface as well as bulk components of $SrRuO_3$ VB spectra and see if the difference between surface and intrinsic electronic structure exists. Finally, by comparing the results that we have obtained using both experimental methods and theoretical approaches, we are able to draw strong conclusions on the degree of electron correlation in this intensively studied perovskite-type material.

II. EXPERIMENT

A. Film deposition, sample characterization, and experimental equipment

Thin $SrRuO_3$ epitaxial film was deposited using reactive dc magnetron sputtering onto a monocrystalline (001)-plane oriented $SrTiO_3$ substrate. Sputtering was performed in an Ar and O_2 mixture (1:1) at a pressure around 15 Pa. To prevent the bombardment of high-energy ions during the deposition, the $SrTiO_3$ substrate was positioned in an "off axis" configuration at a distance of 15 mm from the symmetry axis of the discharge and 20 mm over the target plane. The substrate temperature was set at 600 °C. The thickness of the film was about ∼100 nm. For HAXPES measurements, a fresh *ex situ* sample was used, whereas for UPS measurements, an additional heat treatment was applied to remove the adsorbed surface contaminants. To avoid the surface decomposition at temperatures above ∼250 °C (Ref. 31), the film was cleaned by relatively low ($T \sim 200$ °C) heating under ultrahigh vacuum (UHV) conditions ($P \sim 10^{-10}$ Torr). The completion of the sample degassing process was checked by controlling the UHV system pressure.

The morphology of the film surface was analyzed by standard atomic force microscopy (AFM) in so-called TappingMode™ (SPM D3100/Nanoscope Iva, Veeco). Figure 1 indicates that the surface is composed of atomically flat step-and-terrace structures with root-mean-square roughness $R_q = 0.231$ nm over a scan area of $0.8 \times 0.8\ \mu m^2$. The crystalline structure of the grown film was identified by high-resolution x-ray diffraction (XRD) measurements using Cu $K\alpha$ radiation (Rigaku SmartLab x-ray diffractometer). In θ-2θ scans, only the (00l) peaks of both the $SrTiO_3$ substrate and the $SrRuO_3$ thin film were detected. Typical ω scans of the (002) peak [Fig. 2(b)] show Gaussian-like rocking curves with a full width at half maximum (FWHM) of 0.03°–0.05°. The value of $2\theta = 45.75°$ [Fig. 2(a)] is typical for $SrRuO_3$ thin films grown by pulsed laser deposition (PLD), metal-organic chemical vapor deposition (MOCVD), and dc

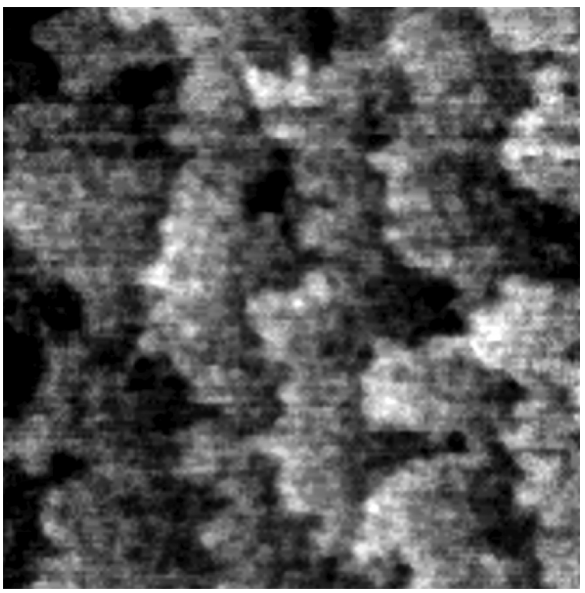

FIG. 1. AFM image of $SrRuO_3$ thin film.

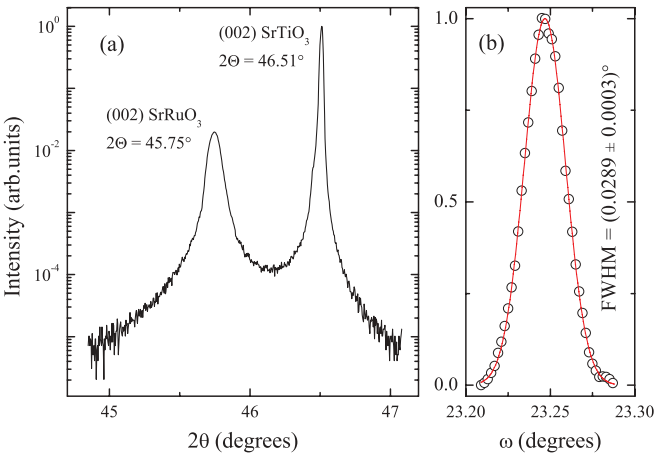

FIG. 2. (Color online) θ-2θ XRD scans (a) and ω-rocking curve (b) of the (002) peak of $SrRuO_3$ thin film.

high pressure sputtering[19,32] and is lower than that $2\theta = 45.96°$ for stoichiometric films.[19] These lattice expansions compared to the parameters of the bulk samples may be attributed to the oxygen and/or ruthenium deficiency of the film.

The temperature dependence of dc resistivity was obtained by a four-probe method. Below Curie temperature (T_c), the experimental data in Fig. 3 have been fitted according to the following equation:[33,34]

$$\varrho(T) = \varrho_0 + AT^n, \tag{1}$$

where ϱ_0 is the residual electrical resistivity at $T = 0$ and A is a constant depending on the properties of the material. We have performed a least-squares fitting for $T < T_c$ and the results are presented as a line in Fig. 3. In the higher temperature region ($T > T_c$), the experimental data have been fitted linearly. The Curie temperature $T_c = 144.9$ K was evaluated from the

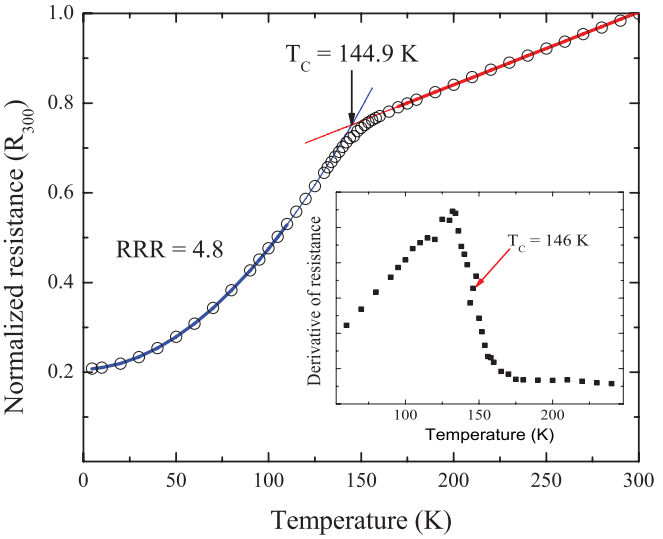

FIG. 3. (Color online) The temperature dependence of $SrRuO_3$ thin film resistance normalized to its value at 300 K. Open circles correspond to experimental data, whereas lines represent the fitted data (see the text for details). Thick lines denote the fitting region. The inset shows the first derivative of resistance.

intersection point of two fitted lines. The residual resistivity ratio RRR = 4.8, defined as the ratio between the resistivity measured at 300 K and at 0 K (ϱ_0 is estimated from the extrapolation of the fitting for $T < T_c$ to 0 K), matches the typical values of about 5 or less reported in the literature for PLD[26,35] and MOCVD[36,37] thin films. Interestingly, the best stoichiometric films prepared by molecular beam epitaxy may exhibit RRR as high as 26 (Ref. 19). The kink in $R(T)$ around T_c shows up as a peak in dR/dT (see inset in Fig. 3) which is usual for metallic ferromagnets. From the derivative of the temperature dependence, we define T_c as the temperature of the midpoint of the jump in dR/dT. This definition gives a value for T_c which is close to the one that was determined using the intersection point. The Curie temperature T_c in bulk samples is 160 K, whereas in our thin film specimen it is reduced by about 15 K. This shift is in agreement with XRD results and may be explained by the presence of lattice strain in the film[34,38] and/or the nonstoichiometry effect.[19]

Resonant UPS experiments were performed in the synchrotron radiation laboratory HASYLAB, Hamburg (Germany). Synchrotron radiation obtained from the storage ring DORIS III was monochromatized with the FLIPPER II plane grating vacuum monochromator, designed for the photon energy range of 15–200 eV. The spectrometer was equipped with a cylindrical mirror electron energy analyzer. The total energy resolution was kept at 0.1 eV. The origin of the energy axis was set at the Fermi level (E_F) as measured for a reference metallic sample. The UPS experiments were done at the normal emission angle, allowing a large solid angle acceptance, which corresponds to an angle-integrated density of states (DOS). The base pressure during UPS measurements was $\sim 10^{-10}$ Torr. To compare our experimental spectra with theoretical band-structure calculations, the data measured were normalized to the photon flux and inelastic backgrounds were removed using the Shirley method.[39]

High-energy HAXPES spectra were measured with the tunable high-energy x-ray photoemission spectrometer at the BW2 beamline (the instrument is equipped with a Scienta SES-200 hemispherical analyzer) in the storage ring DORIS III using an energy resolution of 0.2 eV. The double crystal monochromator Si (111) covers an energy range from 2.4 to 10 keV with a monochromatic photon flux of about 5×10^{12} photons/s and with total energy resolution power of 0.5 eV for a radiation energy of 3000 eV and ~0.9 eV for a radiation energy of 4500 eV. The emission angle α was varied within the range of 8°–90° by rotating the sample (normal emission corresponds to $\alpha = 90°$). The Fermi level position was determined by measuring gold spectra.

B. Resonant UPS data normalization

A set of energy distribution curves (EDCs) of the $SrRuO_3$ thin film normalized to the photon flux energy range covering the Ru $4p \rightarrow 4d$ transition are shown in Fig. 4(a). The second-derivative technique was used to reveal the hidden features of the spectrum [Fig. 4(b)]. The averaging of the second derivative plots over all exciting photon energies was used to minimize data scattering. We note that the feature centered at around 10 eV is known to be due to contaminations, most likely

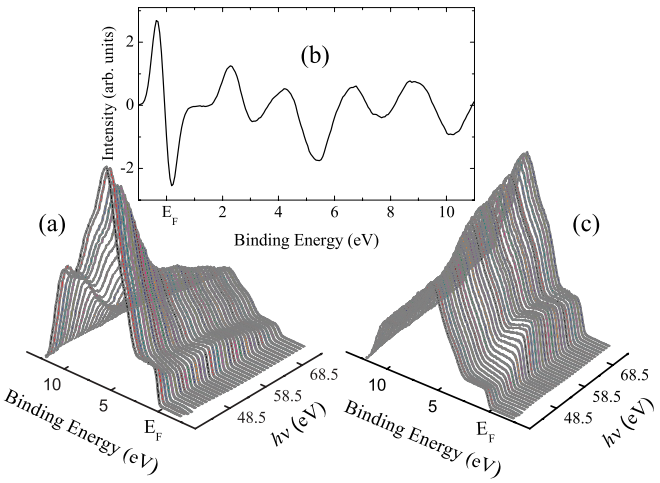

FIG. 4. (Color online) Series of EDCs spectra obtained for various photon energies [(a) and (c)] and the second-derivative plot of an averaged spectra (b). In (a), the spectra were normalized to the photon flux, whereas in (c), the spectra were normalized with respect to the CO-contamination peak (10 eV) intensity.

by carbon monoxide,[15,20] usually present in residual vacuum. Figure 4(c) presents EDCs normalized to CO-contamination peak intensity.

After background subtraction the VB photoemission spectrum for $SrRuO_3$ can be calculated for a particular photon energy using the following approximate expression (DOS approximation):[40–42]

$$I(h\nu, E_B) = n(h\nu)C(E_K) \times [\sigma_{\mathrm{Ru}}(h\nu)D_{\mathrm{Ru}}(E_B) + \sigma_{\mathrm{O}}(h\nu)D_{\mathrm{O}}(E_B) + \sigma_{\mathrm{CO}}(h\nu)D_{\mathrm{CO}}(E_B)]. \quad (2)$$

In this equation, n is the photon flux of the monochromator, E_B is the binding energy (BE), $C(E_K) = \lambda(E_K)T(E_K)$ is the instrumental factor, where λ stands for the inelastic mean-free path of electrons,[43] T is the transmission function of the electron analyzer,[44–46] $E_K = h\nu - E_B - \varphi$ is the kinetic electron energy, and φ denotes the work function of the system, which is a constant of 4.5 eV in our case. D_{Ru} and D_{O} represent the partial DOS (PDOS) for the Ru $4d$ and O $2p$ states, and the respective photoionization cross sections are given by σ_{Ru} and σ_{O}. The third term in Eq. (2) takes into account the localized peak from adventitious carbon monoxide. This peak may be useful for spectra normalization to give almost flat O $2p$ spectral weight in the VB region.[15]

A resonant feature in a constant initial state (CIS) spectrum can be described in terms of the resonant and nonresonant components,[47,48] so

$$\sigma_{\mathrm{Ru}}(h\nu) = \sigma^n_{\mathrm{Ru}}(h\nu)F(\varepsilon). \quad (3)$$

Here $\sigma^n_{\mathrm{Ru}}(h\nu)$ is a slowly varying nonresonant partial cross-section and $F(\varepsilon)$ is the function describing resonant behavior of the photoionization cross section at the Ru $4p \rightarrow 4d$ excitation threshold. The function $F(\varepsilon)$ can be described by a Fano lineshape:[49]

$$F(\varepsilon) = \frac{(\varepsilon + q)^2}{1 + \varepsilon^2}, \quad (4)$$

where $\varepsilon = h(\nu_R - \nu)/w$, $h\nu_R$ is the the Ru $4p \rightarrow 4d$ threshold energy, w describes the spectral width of the autoionized discrete state, and q is the Fano's asymmetry parameter. In order to perform a proper analysis of UPS data, the measured spectra have to be normalized with respect to experimental condition and the general dependence of the photoionization cross sections.[50]

In this work, we use normalization to the contamination peak intensity, i.e., to the last term in Eq. (2) taken at $E_B = E_C$, where $E_C = 10$ eV is the BE corresponding to the contamination peak centroid. Then normalized photoemission spectra intensity I_n can be expressed as follows:

$$I_n(h\nu, E_B) = \frac{C(h\nu - E_B - \varphi)}{C(h\nu - E_C - \varphi)}\left(\frac{\sigma^n_{\mathrm{Ru}}(h\nu)D_{\mathrm{Ru}}(E_B)}{\sigma_{\mathrm{CO}}(h\nu)D_{\mathrm{CO}}(E_C)}F(\varepsilon) + \frac{\sigma_{\mathrm{O}}(h\nu)D_{\mathrm{O}}(E_B)}{\sigma_{\mathrm{CO}}(h\nu)D_{\mathrm{CO}}(E_C)} + \frac{D_{\mathrm{CO}}(E_B)}{D_{\mathrm{CO}}(E_C)}\right). \quad (5)$$

This procedure is reasonable, since this CO-contamination peak arises from the bonding state 5σ of O $2p$ and C $2s/2p$ orbitals in CO, whose photon energy dependence of the cross sections is similar to that of O $2p$.[50–52] Moreover, in the linear approximation such a normalized instrumental factor $C_n(h\nu, E_B) = C(h\nu - E_B - \varphi)/C(h\nu - E_C - \varphi)$ with constant values of E_C and φ becomes independent of the photon energy in the vicinity of the Ru $4p \rightarrow 4d$ resonance. The photon energy is rather limited, therefore it is reasonable to apply a constant instrumental factor. In the used photon energy range, photon energy dependence for the nonresonant photoionization cross section can be approximated by the exponential decay function $\exp(-\chi_i h\nu)$ (Ref. 50), where χ_i is the decay factor and $i =$ Ru, O, and CO. Then Eq. (5) reduces to

$$I_n(h\nu, E_B) = A_{\mathrm{Ru}}e^{-\alpha h\nu}F(\varepsilon)D_{\mathrm{Ru}}(E_B) + A_{\mathrm{O}}e^{-\beta h\nu}D_{\mathrm{O}}(E_B) + A_{\mathrm{CO}}D_{\mathrm{CO}}(E_B), \quad (6)$$

where A_{Ru}, A_{O}, A_{CO}, $\alpha = \chi_{\mathrm{Ru}} - \chi_{\mathrm{CO}}$, and $\beta = \chi_{\mathrm{O}} - \chi_{\mathrm{CO}}$ are constants independent of $h\nu$. This expression was used for further analysis of CIS curves.

III. COMPUTATIONAL DETAILS

In this work, the theoretical calculations were performed with CRYSTAL06 code[53] assuming that the structure of $SrRuO_3$ exhibits orthorhombic $Pbnm$ symmetry. The structural parameters of $SrRuO_3$ were taken from a neutron powder diffraction study.[54] Since CRYSTAL06 code employs a linear combination of atom-centred Gaussian orbitals, in order to avoid numerical problems usually caused by too diffuse valence functions, one has to properly prepare the atomic basis set for crystalline calculations. Concerning the Ru atom, the nonrelativistic pseudopotential (PP) corresponding to 28 core electrons was adopted from the PP library of the Stuttgart/Cologne group.[55] The valence part of this basis set was modified by removing exponents smaller than 0.1 (bohr^{-2}) and optimizing the uncontracted ones. The optimization procedure was based on an attempt to minimize the total energy per unit cell with the lattice constants and atomic positions fixed at the experimental values. For the Sr atom, the small-core Hay-Wadt PP (Ref. 56) was combined with the valence functions from the strontium titanate study.[57] For the O atom, the all-electron basis set originally used to study calcium carbonate was taken from Ref. 58.

Due to the large spatial extent of the $4d$ orbitals, it is natural to expect that the standard DFT model would be a theoretical tool of choice for investigating electronic structure in metallic $SrRuO_3$. As the DFT method is perfectly consistent with the homogeneous electron gas model, it can properly describe the delocalized nature of electrons in the VB. It should be noted that recent studies on $LaNiO_3$[59,60] have revealed the ability of pure DFT to reproduce the VB features in less extended and hence more correlated $3d$ transition metal systems. Thus, the calculations presented in this paper were made using the generalized gradient approximation (GGA) within the DFT framework. The choice of exchange-correlation functional suggested by Perdew, Burke, and Ernzerhof[61] (PBE) is based on the fact that this version of GGA does not contain any parameter that was determined to reproduce experimental or precise *ab initio* data.[62] Since the PBE functional represents a well tempered balance between computational efficiency, numerical accuracy, and reliability,[63] it is considered as a standard functional for solid-state calculations.[64] The reciprocal space was sampled according to a regular sublattice with a shrinking factor of 12 that corresponds to 343 independent k points in the irreducible Brillouin zone. In order to improve the self-consistence field convergence, the Kohn-Sham matrix mixing technique (keyword FMIXING) and Anderson's method,[65] as proposed by Hamann[66] (keyword ANDERSON), were applied. The default values of the truncation tolerances for bielectronic integrals were modified to 9 9 9 9 18 (keyword TOLINTEG) and the tolerance on change in total energy was set to 10 (keyword TOLDEE) (for more details see CRYSTAL06 User's Manual[53]).

IV. RESULTS AND DISCUSSION

A. Theoretical calculations

The calculated DOS of $SrRuO_3$, shown in Fig. 5, reveals that the VB is essentially formed by strongly hybridized O $2p$ and

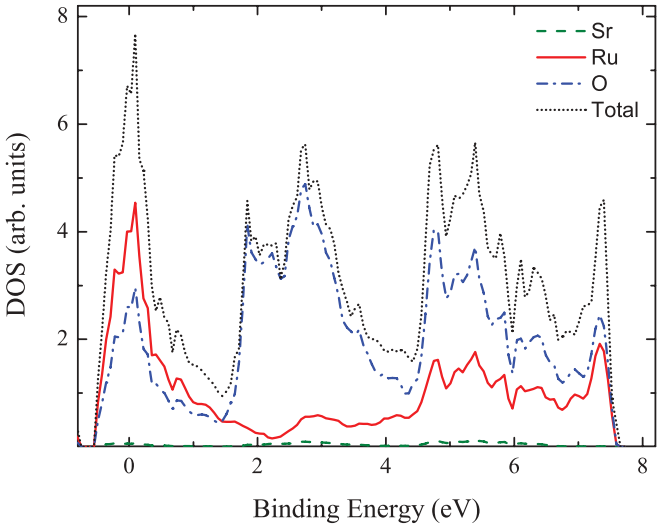

FIG. 5. (Color online) The total and partial DOS of $SrRuO_3$ calculated using the PBE exchange-correlation functional. The Fermi energy is set at zero.

TABLE I. Mulliken atomic charges $Q(e)$ and overlap populations $OP(e)$ with respect to the O atom.

Quantity	Sr	Ru	O
Q	1.834	0.984	−0.952
OP	−0.026	0.108	−0.138

Ru 4*d* orbitals. It is clearly seen that the sharp peak at the Fermi energy is dominated by Ru 4*d* character. This result is nicely consistent with previous plane-wave and muffin-tin[27–30] DFT calculations demonstrating high reliability from a theoretical perspective.

A strong hybridization between O 2*p* and Ru 4*d* orbitals is also reflected in the Mulliken population analysis and electron-density difference map, presented in Table I and Fig. 6, respectively. Although this type of analysis is basis set dependent, it indicates a significant covalent contribution to the Ru-O chemical bond, since atomic charges for Ru ($+0.984e$) and O ($-0.952e$) atoms substantially differ from formal ionic picture of Ru^{4+} and O^{2-}. Interestingly, the Sr ($+1.834e$) atom retains most of its ionic character of Sr^{2+}. The electron-density difference map, obtained by subtracting the superposition of spherical atomic charge distributions from the crystal electron density, confirms a significant and much weaker covalent part in chemical bonding for Ru-O and Sr-O atoms, respectively. As can be seen from Fig. 6, the electron density considerably increases at the O atom in the Sr-O bond direction, whereas the Sr atom is mainly surrounded by negative isolines, implying that the Sr-O bond has predominantly ionic character. The decrease in electron density at both Ru and O atoms eventually replaced by a tight concentration of positive isolines within the Ru-O bond reveals a large degree of covalency in the Ru-O bond.

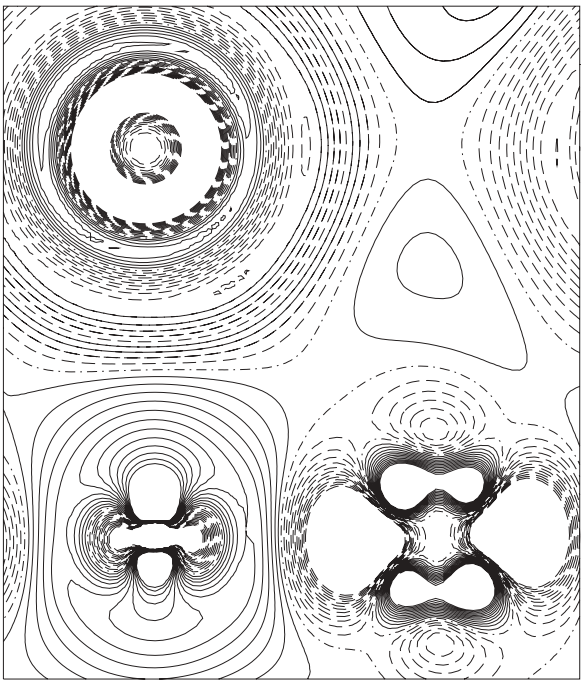

FIG. 6. The electron-density difference map for $SrRuO_3$. Continuous, dashed, and dotted-dashed isolines represent positive, negative, and zero value differences of density, respectively. Sr, Ru, and O atoms are located at the top left, bottom right, and bottom left corners of the map, respectively. The isolines are drawn from −0.03 to 0.03 e/bohr^3 with a step of 0.0025 e/bohr^3.

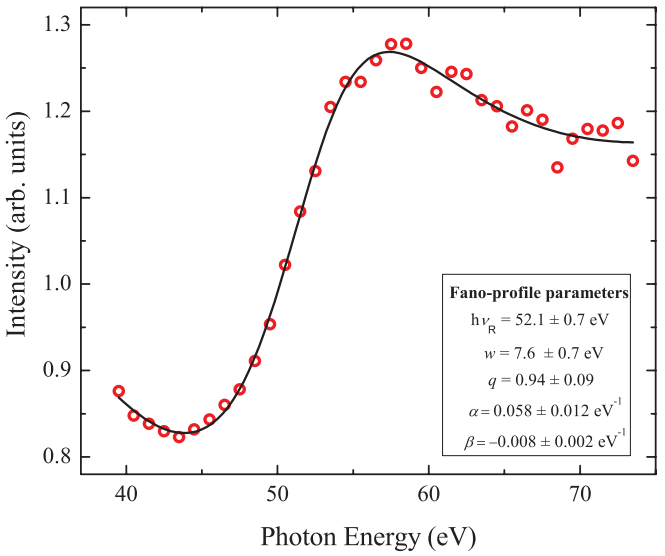

FIG. 7. (Color online) Fano resonance of the Ru 4*d* states gap ($E_F - 7.8$ eV) calculated from the spectra presented in Fig. 4(c).

B. Resonant ultraviolet photoemission spectra

Concerning UPS data analysis, in order to prove the occurrence of the Ru $4p \rightarrow 4d$ resonance, the VB spectra have been integrated in the BE range of $E_F - 7.8$ eV and are shown in Fig. 7 as a function of photon energy. Theoretically, the data can be described well using a Fano profile combined with an inherent nonresonant background [Eq. (6)], with a threshold energy $h\nu_R = 52.1$ eV, a width of the resonance $w = 7.6$ eV, and an asymmetry factor $q = 0.94$ (see Fig. 7). The obtained value of the resonance energy $h\nu_R = 52.1 \pm 0.7$ eV agrees with the published data.[14,15] One should note that our cross-section decay factor $\alpha = 0.058 \pm 0.012$ eV^{-1} is in a good agreement with $\chi_{Ru} - \chi_{CO} \approx 0.05$ eV estimated from theoretically calculated cross-section dependencies.[50] The relatively large linewidth of a resonance ($w \sim 8$ eV) is consistent with the expectation that the 4*d* orbital is pretty extended and hence the bonding with the O 2*p* orbitals is strong. Using this plot, the on-resonance energy is determined to be $h\nu_{on} \approx 59.5$ eV, while off-resonance energy is determined to be $h\nu_{off} \approx 45.5$ eV.

In principle, resonance in photoemission allows one to estimate the contribution of the Ru 4*d* shell to the DOS in VB. In particular, a difference between EDCs taken for photon energies corresponding to the on-resonance energy and off-resonance energy should provide the PSW. However, this is only true if the variation in O 2*p* cross sections [the second term in Eq. (6)] can be neglected. In cases of weak and broad resonance, variations of nonresonating oxygen cross sections may be comparable with the effect of Ru $4p \rightarrow 4d$ resonance and thus may significantly distort the results, especially if the admixture of O 2*p* states is strong.

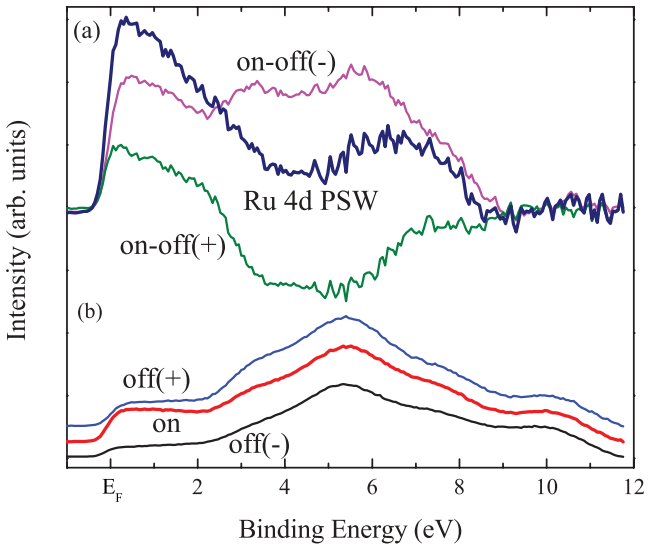

FIG. 8. (Color online) (a) Ru 4*d* PSW obtained from equidistant difference spectra at on–off(−) and on–off(+) resonance conditions. (b) EDCs spectra obtained for photon energies $h\nu = 45.5$, 59.5, and 73.5 eV for off(−), on, and off(+) resonance conditions, respectively. The EDC spectra were normalized to the contamination peak (10 eV) intensity [see Fig. 4(b)].

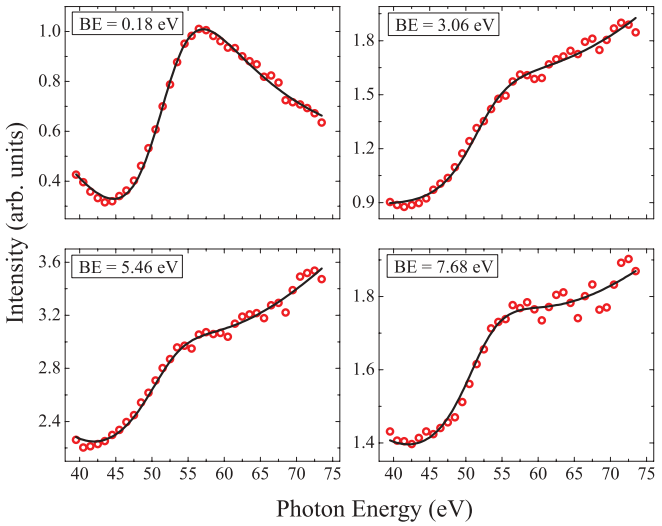

FIG. 9. (Color online) The Fano-profile CIS spectra of $SrRuO_3$ thin film measured at BE corresponding the second derivative minima in the EDC spectra [see Fig. 4(b)].

This can be easily seen by comparing equidistant spectra measured around the Fano-profile maximum. Figure 8 presents the EDCs of a $SrRuO_3$ thin film measured at the maximum of the Fano profile (on resonance: $h\nu_{on} = 59.5$ eV) and two equidistant photon energies [off(−) and off(+): $h\nu^{-}_{off} = 45.5$ and $h\nu^{+}_{off} = 73.5$ eV, respectively]. Strong resonant behavior occurs at BE < 2 eV in agreement with the Ru 4*d* character of PDOS at these energies (see Fig. 5). An appreciable discrepancy between the on–off(−) and on–off(+) spectra at BE > 2 eV (i.e., in the region where O 2*p* states form the largest contribution to the VB) clearly shows that oxygen cross-section dependence on the photon energy considerably affects the shape of difference spectra, therefore they cannot be directly used for Ru 4*d* PSW estimations. On the other hand, the $h\nu$ dependence of the second term in Eq. (6) is relatively low ($\beta = -0.008$ eV^{-1}), while the $h\nu$ interval of interest is rather limited (59.5 ± 14 eV) and within the first approximation $\exp(-\beta h\nu)$ in Eq. (6) may be replaced by $\exp(-\beta h\nu) \sim [1 - \beta h(\nu - \nu_{on})]$.

Taking into account this linear approximation, the equidistant difference spectrum, i.e., $I_{Diff}(E_B) = I_n(h\nu_{on}, E_B) - [I_n(h\nu^{-}_{off}, E_B) + I_n(h\nu^{+}_{off}, E_B)]/2$, only contains the resonantly enhanced Ru 4*d* contribution, while the last two terms, representing the oxygen and CO-contamination contribution to the VB spectra, annihilate. Thus, the constructed Ru 4*d* PSW is shown in Fig. 8. We note, that the precise selection of $h\nu_{on}$ and $(h\nu_{on} - h\nu^{-}_{off}) = (h\nu^{+}_{off} - h\nu_{on})$ is not critical for determining $D_{Ru}(E_B)$ and affects only the magnitude of difference spectra.

Another more proper way to obtain $D_{Ru}(E_B)$ is to fit VB CIS spectra at various BEs with a model function of Eq. (6). As an example, in Fig. 9 we show fitted CIS spectra measured at a BE corresponding to the VB features [see Fig. 4(b)]. It is evident that at BE $\gtrsim 2$ eV O 2*p* states significantly contribute to the VB, and Fano-profile parameters cannot be determined with sufficient accuracy. That is the reason why we use parameters $h\nu_R$, w, and q determined earlier (Fig. 7) for curve fitting. Figure 10 shows the Ru 4*d* PSW of the $SrRuO_3$ VB obtained from equidistant EDC spectra and Fano-profile fitting of CIS curves in comparison with theoretical calculations.

As can be seen from Fig. 10, experimentally and theoretically obtained Ru 4*d* states spread over a wide energy range and are in a good qualitative accordance with each other. One can also notice that the intense Ru 4*d* coherent part of the spectra near the Fermi level is clearly identified in our experimentally extracted Ru 4*d* PSW. This result makes us believe that a spectral weight transfer from a coherent to an incoherent feature, previously observed with *ex situ* specimens,[9,13–16] could be eliminated by applying an advanced handling of experimental data and/or relevant preparation of samples. As was suggested by Kim *et al.*,[20] thin films grown *in situ* and thus free of additional surface cleaning may provide the best opportunity to employ PES for studying the intrinsic electronic structure of $SrRuO_3$. Indeed, *in situ* prepared specimens have exhibited noticeably sharper Ru 4*d* PSWs at the Fermi level,[19,20] supporting the idea that the absence of coherent feature of the spectra—which is taken as a proof of strong electron correlation in $SrRuO_3$—could be originated by the contribution from the affected electronic structure at the surface. It should be noted that less surface-sensitive x-ray PES measurements have also revealed clearly pronounced Ru 4*d* peak at the Fermi level.[21–24] For all these reasons, we strongly believe that electronic structure of $SrRuO_3$ can be successfully described by standard DFT approximation, since in this material VB electrons are delocalized and therefore self-interaction errors are negligible. The absence of coherent feature of the spectra indicating the localized electronic states could be attributed to external factors, for example, surface roughness, defects, or change of the symmetry that may occur during the growth and/or cleaning process. In order to capture the physics of such a surface affected system, one should apply something beyond the DFT framework, for

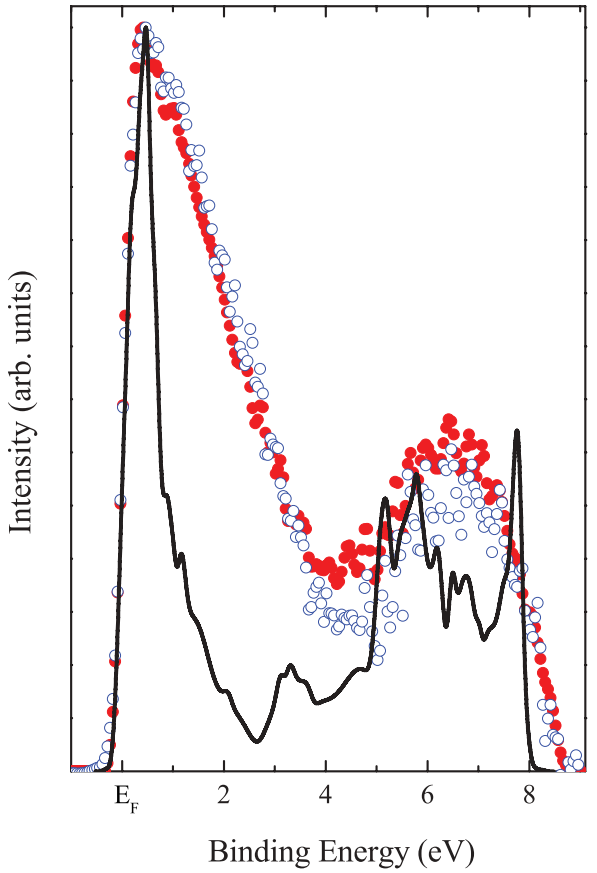

FIG. 10. (Color online) The comparison of theoretically calculated (solid line) Ru 4*d* PDOS with experimentally obtained from Fano-profile fitting of CIS spectra (filled circles) and the EDCs equidistant difference spectra (open circles) Ru 4*d* PSW. Theoretical calculations were convoluted with Gaussian functions (FWHM = 0.1 eV).

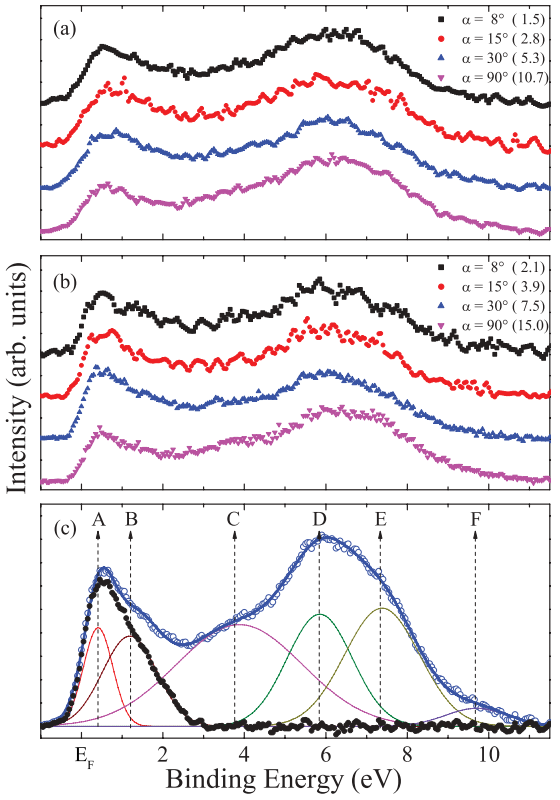

FIG. 11. (Color online) The set of VB spectra normalized to the integrated intensity for different emission angles measured at (a) $h\nu = 3000$ eV and (b) $h\nu = 4500$ eV. (c) Fitted cumulative spectrum. The values in brackets are the escape depths in ML. In (c), open circles correspond to the raw data, the thick line is the spectral envelope, thin lines are the spectral components, and filled circles represent the dominant Ru 4*d* region after removing the contribution from higher BE states.

instance, self-interaction corrected (SIC) DFT, DFT + U, or a dynamical mean-field theory (DMFT) approach.

C. High-energy angle-resolved photoemission spectra

In order to see how the Ru 4*d* PSW changes along the depth of the film, we have examined the angle and photon energy dependence of HAXPES spectra (see Fig. 11). According to Refs. 67, 68, and 69, the mean free paths at $h\nu = 3000$ and 4500 eV are $\lambda_{3000} = 10.7$ monolayers (ML) and $\lambda_{4500} = 15$ ML, respectively.

Figure 11(c) shows a cumulative plot of the VB obtained by averaging spectra measured at different collection angles and photon energies. The spectrum was fitted with six Gaussian peaks, thus the VB exhibits six distinct features marked by A, B, C, D, E, and F. Our theoretical calculations as well as some previous studies[9,13,14,30] reveal that the band between E_F and ~2 eV is mainly composed of Ru 4*d* states, whereas O 2*p* states become dominant in the region of 2–4 eV (C). The sharp peak near the Fermi level (A) and the broad one centered at ~1.2 eV (B) are usually assigned to the coherent and incoherent parts of the spectral function, respectively.[9,14,25] The peaks D and E can be attributed to the mixture of Ru 4*d* and O 2*p* orbitals. The finite emission at 8–11 eV (negligible peak F) is due to the contaminations.

At higher (>300 eV) photon energies, the photoionization cross section of O 2*p* electrons decreases more rapidly than that of Ru 4*d* electrons. For example, the atomic calculations predict Ru 4*d*/O 2*p* cross-section ratios of 36 and 74 for $h\nu = 1500$ and 8047.8 eV, respectively.[50,70] Rough interpolation provides Ru 4*d*/O 2*p* cross-section ratios of 50 for $h\nu = 3000$ eV and 60 for $h\nu = 4500$ eV. In solids, due to the hybridization between O 2*p* and Ru 4*d* orbitals these values somewhat decrease, but despite that Ru 4*d* states should form the main part of photoemission spectra measured in the vicinity of the Fermi level. This becomes evident when spectra presented in Fig. 11 are compared to the spectra measured at low (~60 eV) photon energies (see Fig. 4) with a Ru 4*d*/O 2*p* cross-section ratio of ≈ 1.1 (Ref. 50). In fact, the spectra in Fig. 11 provide a qualitative picture of the Ru 4*d* PSW at low (< 2 eV) BE where Ru 4*d* states occupy the largest part of the VB. This result is in agreement with the Ru 4*d* PSW extracted from resonant UPS measurements (see Fig. 10). At higher BE, the O 2p contribution cannot be neglected, since theoretical calculations show that the intensity of O 2*p* states substantially increases compared to the intensity of Ru 4*d* states.

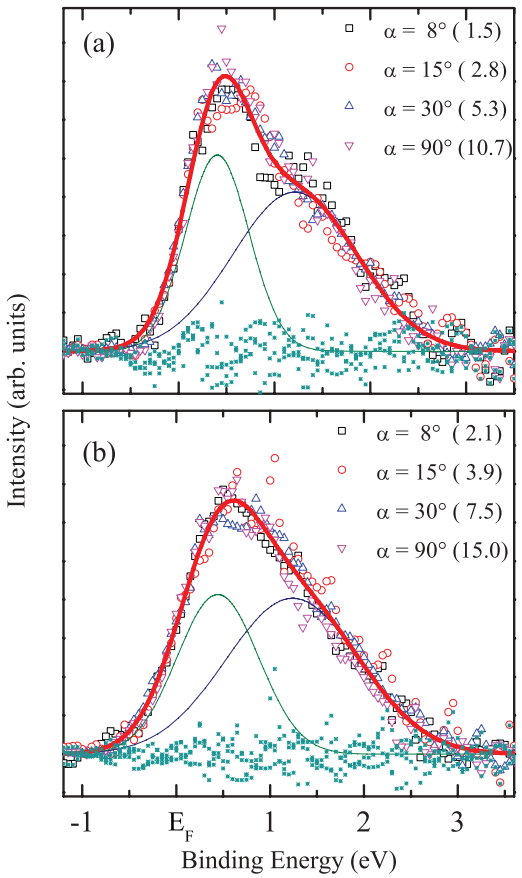

FIG. 12. (Color online) Ru 4*d* spectra from (a) $h\nu = 3000$ eV and (b) $h\nu = 4500$ eV measurements after the subtraction of the O 2*p* contribution from higher BE states [see Fig. 11(c)]. The values in brackets are the photoelectron escape depths in ML. Open symbols correspond to the raw data, the thick line is the spectral envelope, thin lines are the spectral components, and points are the residuals.

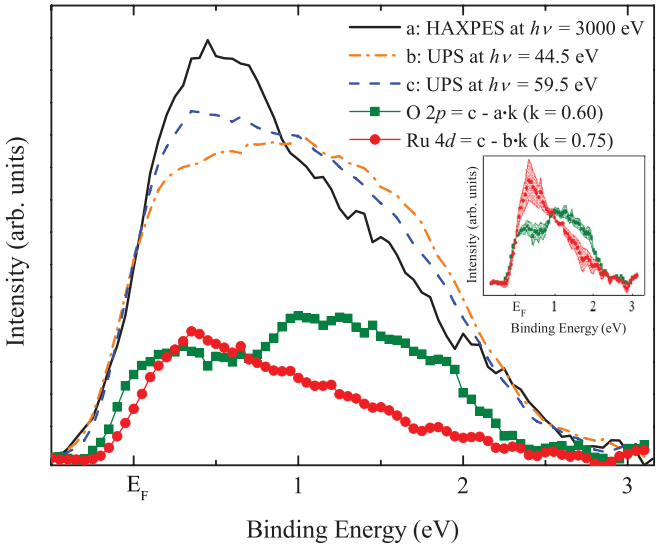

FIG. 13. (Color online) Comparison of normalized photoemission spectra in the dominant Ru 4d region obtained at on-resonance ($h\nu = 59.5$ eV) and off-resonance ($h\nu = 44.5$ eV) conditions with a high-energy spectrum measured at grazing emission ($\alpha = 8^\circ$). Squares correspond to the appropriately weighted difference between on-resonance and high-energy spectra and circles to the difference between on-resonance and off-resonance spectra. k is the weighting factor used in the estimation. The inset reveals how the variation of k by ± 0.1 is reflected in the difference spectra.

In order to obtain the approximate bulk and surface components of the Ru 4*d* band, we have subtracted the O 2*p* contribution following the procedure of Refs. 11 and 23 [see Fig. 11(c)]. The obtained Ru 4*d* spectra were normalized to the integrated intensity and are shown in Fig. 12. It is widely assumed that the coherent feature at ~0.4 eV corresponds to the delocalized DOS reproduced by *ab initio* calculations, whereas the incoherent feature at ~1.2 eV should be attributed to the presence of localized electronic states. One may also expect the increase of the incoherent component with decreasing escape depth. However, we demonstrate that the shape of Ru 4*d* band is actually independent of the emission angle and excitation energy. The broader Fermi cutoff and the widening of synthetic components at $h\nu = 4500$ eV can be attributed to the lower resolution at this photon energy. This result provides a strong proof that contribution from the coherent and incoherent features does not vary with increasing photoelectron escape depth L from ~1.5 ML ($h\nu = 3000$ eV, $\alpha = 8^\circ$) to ~15 ML ($h\nu = 4500$ eV, $\alpha = 90^\circ$). Moreover, only a weak shoulder was observed at ~1.2 eV.

This is somewhat surprising, since in the literature one can find some evidence that bulk and surface components deduced from the angle and $h\nu$ dependences of the PES spectra significantly differ, with incoherent states dominating at the surface.[9,11,12,22,23] Our results show that high photon energy and low emission angle ($\alpha = 8^\circ$, $L \sim 1.5$, and 2.1 ML at $h\nu =$ 3000 and 4500 eV, respectively) HAXPES spectra represent the intrinsic ($\alpha = 90^\circ$, $L \sim 10.7$ and 15 ML at $h\nu = 3000$ and 4500 eV, respectively) $SrRuO_3$ electronic structure, with coherent Ru 4*d* states remaining dominant at the surface. These spectra are in agreement with the Ru 4*d* PSW obtained from more surface-sensitive [$\lambda_{60} \sim 2$ ML (Ref. 68)] resonant UPS measurements (see Fig. 10). It should be noted that some care must be taken when comparing spectra obtained at different photon energies, since an increase in $h\nu$ causes the growth of both the escape depth and the Ru 4*d*/O 2*p* cross-section ratio.

Interestingly, O 2*p* states provide a finite contribution to the theoretical spectrum even in the region dominated by Ru 4*d* electrons (see Fig. 5), thus some admixture of O 2*p* states should also be visible in the experiments. Figure 13 illustrates the significance of this effect on Ru 4*d* spectra obtained at particularly different photon energies which are characterized by very close escape depth.

An increase in intensity around ~1.2 eV with decreasing photon energy is usually explained in terms of different surface and bulk electronic structures.[9,11,12,23] In our case, however, both resonant UPS and HAXPES spectra presented in Fig. 13 were obtained from approximately the same depth of the sample [for resonant UPS, escape depth is ~2 ML (Ref. 71) or ~1.1 ML (Ref. 67), whereas for HAXPES measurements it is ~1.9 ML (Ref. 71) or ~1.5 ML (Ref. 67)]. For this reason, the apparent difference in the spectra cannot be attributed to the localized Ru 4*d* surface states and should be related to a finite contribution from O 2*p* states. The difference between

on-resonance and high-energy spectra provides a qualitative picture of the O $2p$ PSW in the dominant Ru $4d$ region. This result agrees with data presented in Ref. 14. We would like to stress that the obtained O $2p$ PSW possesses a maximum at ∼1.2 eV, i.e., at the location of incoherent feature. In Fig. 13, the off-resonance part of the spectra has no significant features near the Fermi level. It demonstrates an agreement with predictions from Fano model [see Eq.(4)], since at this photon energy the Ru $4d$ contribution vanishes and only O $2p$ states form the photoemission spectra. The difference between on-resonance and off-resonance spectra provides a Ru $4d$ PSW which fairly well matches the theoretical calculations (Fig. 5). We can conclude that the incoherent component of the spectrum located at ∼1.2 eV is observed at least partially due to the admixture of O $2p$ states in the dominant Ru $4d$ region. In order to see the influence of the uncertainties related to the weighting factor k, we have added an inset in Fig. 13.

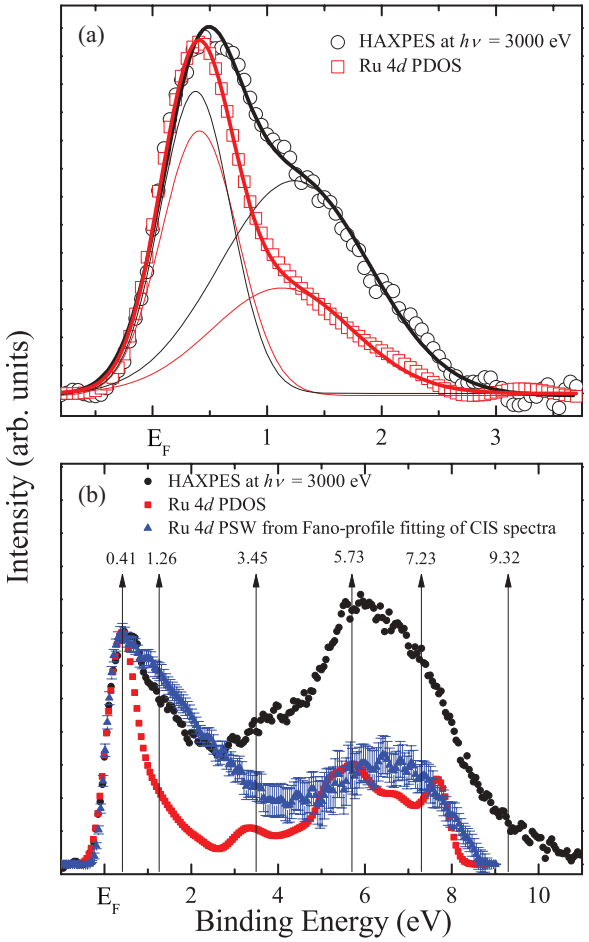

FIG. 14. (Color online) (a) Comparison of convoluted DFT results with the spectrum measured at $h\nu = 3000$ in the dominant Ru $4d$ region (see Fig. 12). Thin lines represent the spectral components and thick lines are the spectral envelopes. (b) Comparison of VB spectra measured at $h\nu = 3000$ eV with the Ru $4d$ PSW extracted from resonant UPS measurements and the convoluted DFT results. Arrows represent the positions of spectral components (in eV) obtained by fitting cumulative HAXPES spectra at $h\nu = 3000$ eV. Error bars show the confidence interval at 95% level, i.e., twice the standard error.

It shows how the variation of the weighting factor's nominal value by ±0.1 (filled band) changes the difference spectra. One can remark that both spectra presented in the inset do not change their lineshapes appreciably. Therefore, we consider that the obtained difference spectra indeed represent the O $2p$ and Ru $4d$ contributions to the VB of $SrRuO_3$.

It is worth mentioning that despite the absence of an incoherent feature in the DFT results, the asymmetric shape of coherent feature may also provide some contribution to the Ru $4d$ PSW in the vicinity of incoherent peak. In order to directly compare theoretical Ru $4d$ PDOS with the experimental measurements made at $h\nu = 3000$ eV, DFT results were convoluted with Gaussian functions (FWHM = 0.5 eV). Spectra normalized to the integrated intensity are shown in Fig. 14 which demonstrates that, although the localized states are not present in DFT calculations, a significantly broad component (∼40% of total intensity) arises in the convoluted Ru $4d$ PDOS at BE corresponding the reported data of the incoherent peak position.[9,14,25] It can be concluded that both the finite admixture of O $2p$ states in the dominant Ru $4d$ region and the asymmetric shape of the coherent Ru $4d$ feature, also obtained in some previous theoretical studies,[14,25,28,30] may contribute to the experimentally observed broad incoherent feature at ∼1.2–1.5 eV, thus suppressing the relative importance of localized surface states.

V. CONCLUSIONS

To summarize, the correlation effects in $SrRuO_3$ thin films were studied experimentally and theoretically by means of resonant UPS, angle-resolved HAXPES, and LCAO approaches within a DFT GGA framework. The employment of two resonant UPS data analysis methods, Fano-profile fitting of CIS spectra and EDC equidistant difference spectra, reveals that the Ru $4d$ PSW has a clear coherent feature in the vicinity of the Fermi level. As this result is in contrast with previously reported UPS spectra from *ex situ* prepared specimens and fairly well agrees with UPS measurements from *in situ* grown thin films, we believe that a shift in the spectral weight towards the incoherent Ru $4d$ peak may be removed by applying an improved handling of experimental data and/or relevant sample preparation techniques. The angle-resolved HAXPES measurements show that surface and bulk components of Ru $4d$ spectra do not differ and, what is more, the comparison with theoretical calculations and resonant UPS data indicate that manifestation of an incoherent peak as a shoulder could be due to the asymmetric shape of a coherent feature and finite admixture of O $2p$ states. These results allow us to conclude that $SrRuO_3$ is a weakly correlated material, therefore the physics of this perovskite can be captured using standard *ab initio* methods.

ACKNOWLEDGMENTS

This work was partially supported by DESY and the European Commission under Grant Agreement ELISA 226716, IA-SFS Project No. DESY-D-I-20100305 EC. Š.M. gratefully acknowledges the Research Council of Lithuania.

*segre@pfi.lt
†Sarunas.Masys@tfai.vu.lt
‡sigism@pfi.lt
§lisa@pfi.lt
|Valdas.Jonauskas@tfai.vu.lt

[1] B. J. Kennedy, B. A. Hunter, and J. R. Hester, Phys. Rev. B **65**, 224103 (2002).
[2] F. He, B. O. Wells, Z.-G. Ban, S. P. Alpay, S. Grenier, S. M. Shapiro, W. Si, A. Clark, and X. X. Xi, Phys. Rev. B **70**, 235405 (2004).
[3] M. Stengel and N. A. Spaldin, Nature (London) **443**, 679 (2006).
[4] S. C. Gausepohl, M. Lee, L. Antognazza, and K. Char, Appl. Phys. Lett. **67**, 1313 (1995).
[5] K. S. Takahashi, A. Sawa, Y. Ishii, H. Akoh, M. Kawasaki, and Y. Tokura, Phys. Rev. B **67**, 094413 (2003).
[6] T. Fujii, M. Kawasaki, A. Sawa, H. Akoh, Y. Kawazoe, and Y. Tokura, Appl. Phys. Lett. **86**, 012107 (2005).
[7] R. Ramesh and N. A. Spaldin, Nat. Mater. **6**, 21 (2007).
[8] G. Koster, L. Klein, W. Siemons, G. Rijnders, J. S. Dodge, C.-B. Eom, D. H. A. Blank, and M. R. Beasley, Rev. Mod. Phys. **84**, 253 (2012).
[9] K. Maiti and R. S. Singh, Phys. Rev. B **71**, 161102 (2005).
[10] I. I. Mazin and D. J. Singh, Phys. Rev. B **56**, 2556 (1997).
[11] K. Maiti, R. S. Singh, and V. R. R. Medicherla, Phys. Rev. B **76**, 165128 (2007).
[12] R. S. Singh, V. R. R. Medicherla, and K. Maiti, Physica B **403**, 1398 (2008).
[13] J. Okamoto, T. Mizokawa, A. Fujimori, I. Hase, M. Nohara, H. Takagi, Y. Takeda, and M. Takano, Phys. Rev. B **60**, 2281 (1999).
[14] K. Fujioka, J. Okamoto, T. Mizokawa, A. Fujimori, I. Hase, M. Abbate, H. J. Lin, C. T. Chen, Y. Takeda, and M. Takano, Phys. Rev. B **56**, 6380 (1997).
[15] J. Park, S.-J. Oh, J.-H. Park, D. M. Kim, and C.-B. Eom, Phys. Rev. B **69**, 085108 (2004).
[16] M. Rao, V. Sathe, D. Sornadurai, B. Panigrahi, and T. Shripathi, J. Phys. Chem. Solids **62**, 797 (2001).
[17] S. Grebinskij, M. Senulis, H. Tvardauskas, V. Bondarenka, V. Lisauskas, B. Vengalis, B. Orlowski, R. Johnson, and S. Mickevičius, Radiat. Phys. Chem. **80**, 1140 (2011).
[18] H. Hadipour and M. Akhavan, Eur. Phys. J. B **84**, 203 (2011).
[19] W. Siemons, G. Koster, A. Vailionis, H. Yamamoto, D. H. A. Blank, and M. R. Beasley, Phys. Rev. B **76**, 075126 (2007).
[20] J. Kim, J. Chung, and S.-J. Oh, Phys. Rev. B **71**, 121406 (2005).
[21] K. Horiba, H. Kawanaka, Y. Aiura, T. Saitoh, C. Satoh, Y. Kikuchi, M. Yokoyama, Y. Nishihara, R. Eguchi, Y. Senba, H. Ohashi, Y. Kitajima, and S. Shin, Phys. Rev. B **81**, 245127 (2010).
[22] H. Kumigashira, M. Minohara, M. Takizawa, A. Fujimori, D. Toyota, I. Ohkubo, M. Oshima, M. Lippmaa, and M. Kawasaki, Appl. Phys. Lett. **92**, 122105 (2008).
[23] M. Takizawa, D. Toyota, H. Wadati, A. Chikamatsu, H. Kumigashira, A. Fujimori, M. Oshima, Z. Fang, M. Lippmaa, M. Kawasaki, and H. Koinuma, Phys. Rev. B **72**, 060404 (2005).
[24] D. Toyota, I. Ohkubo, H. Kumigashira, M. Oshima, T. Ohnishi, M. Lippmaa, M. Takizawa, A. Fujimori, K. Ono, M. Kawasaki, and H. Koinuma, Appl. Phys. Lett. **87**, 162508 (2005).
[25] J. M. Rondinelli, N. M. Caffrey, S. Sanvito, and N. A. Spaldin, Phys. Rev. B **78**, 155107 (2008).
[26] A. Vailionis, W. Siemons, and G. Koster, Appl. Phys. Lett. **93**, 051909 (2008).
[27] K. Maiti, Phys. Rev. B **77**, 212407 (2008).
[28] K. Maiti, Phys. Rev. B **73**, 235110 (2006).
[29] P. Mahadevan, F. Aryasetiawan, A. Janotti, and T. Sasaki, Phys. Rev. B **80**, 035106 (2009).
[30] J. Manica, M. Abbate, J. Gayone, J. Guevara, and S. Cuffini, J. Alloys Compd. **377**, 25 (2004).
[31] J. Shin, S. Kalinin, H. Lee, H. Christen, R. Moore, E. Plummer, and A. Baddorf, Surf. Sci. **581**, 118 (2005).
[32] M. Mlynarczyk, K. Szot, A. Petraru, U. Poppe, U. Breuer, R. Waser, and K. Tomala, J. Appl. Phys. **101**, 023701 (2007).
[33] Y. Liu, R. Jin, Z. Q. Mao, K. D. Nelson, M. K. Haas, and R. J. Cava, Phys. Rev. B **63**, 174435 (2001).
[34] S. B. Anooz, J. Schwarzkopf, R. Dirsyte, M. Schmidbauer, K. Irmscher, A. Kwasniewski, and R. Fornari, Mater. Sci. Eng. B **176**, 647 (2011).
[35] X. D. Wu, S. R. Foltyn, R. C. Dye, Y. Coulter, and R. E. Muenchausen, Appl. Phys. Lett. **62**, 2434 (1993).
[36] K. Takahashi, T. Oikawa, K. Saito, H. Fujisawa, M. Shimizu, and H. Funakubo, Jpn. J. Appl. Phys. **41**, 6873 (2002).
[37] J. Choi, Y. Choi, J. Hong, H. Tian, J. Roh, Y. Kim, T. Chung, Y. Oh, Y. Kim, C. Kim, and K. No, Jpn. J. Appl. Phys. **41**, 6852 (2002).
[38] Q. Gan, R. A. Rao, C. B. Eom, J. L. Garrett, and M. Lee, Appl. Phys. Lett. **72**, 978 (1998).
[39] D. A. Shirley, Phys. Rev. B **5**, 4709 (1972).
[40] W. Braun, A. Goldmann, and M. Cardona, Phys. Rev. B **10**, 5069 (1974).
[41] S. Laubach, P. C. Schmidt, A. Thissen, F. J. Fernandez-Madrigal, Q.-H. Wu, W. Jaegermann, M. Klemm, and S. Horn, Phys. Chem. Chem. Phys. **9**, 2564 (2007).
[42] D. Brown, M. Crapper, K. Bedwell, L. Flannery, M. Petty, and P. Skull, J. Phys.: Condens. Matter **8**, 5941 (1996).
[43] S. Tanuma, C. J. Powell, and D. R. Penn, Surf. Interface Anal. **17**, 911 (1991).
[44] D. Briggs and J. T. Grant, *Surface Analysis by Auger and X-ray Photoelectron Spectroscopy* (IM Publications and Surface Spectra Limited, Chichester, UK, 2003).
[45] T. Loher, A. Klein, C. Pettenkofer, and W. Jaegermann, J. Appl. Phys. **81**, 7806 (1997).
[46] J. Ghijsen, L. H. Tjeng, H. Eskes, G. A. Sawatzky, and R. L. Johnson, Phys. Rev. B **42**, 2268 (1990).
[47] L. C. Davis and L. A. Feldkamp, Phys. Rev. B **23**, 6239 (1981).
[48] P. H. Kobrin, U. Becker, S. Southworth, C. M. Truesdale, D. W. Lindle, and D. A. Shirley, Phys. Rev. A **26**, 842 (1982).
[49] U. Fano, Phys. Rev. **124**, 1866 (1961).
[50] J. J. Yeh and I. Lindau, At. Data Nucl. Data Tables **32**, 1 (1985).
[51] I. Wilhelmy, L. Ackermann, A. Gorling, and N. Risch, J. Chem. Phys. **100**, 2808 (1994).
[52] E. W. Plummer, T. Gustafsson, W. Gudat, and D. E. Eastman, Phys. Rev. A **15**, 2339 (1977).
[53] R. Dovesi, V. R. Saunders, C. Roetti, R. Orlando, C. M. Zicovich-Wilson, F. Pascale, B. Civalleri, K. Doll, N. M. Harrison, I. J. Bush, P. D'Arco, and M. Llunell, CRYSTAL06 *User's Manual* (University of Torino, Torino, 2006).
[54] B. J. Kennedy and B. A. Hunter, Phys. Rev. B **58**, 653 (1998).
[55] http://www.theochem.uni-stuttgart.de/pseudopotentials/clickpse.en.html
[56] P. J. Hay and W. R. Wadt, J. Chem. Phys. **82**, 299 (1985).
[57] S. Piskunov, E. Heifets, R. Eglitis, and G. Borstel, Comput. Mater. Sci. **29**, 165 (2004).

[58]L. Valenzano, F. J. Torres, D. Klaus, F. Pascale, C. M. Zicovich-Wilson, and R. Dovesi, Z. Phys. Chem. **220**, 893 (2006).
[59]Š. Masys, S. Mickevičius, S. Grebinskij, and V. Jonauskas, Phys. Rev. B **82**, 165120 (2010).
[60]G. Gou, I. Grinberg, A. M. Rappe, and J. M. Rondinelli, Phys. Rev. B **84**, 144101 (2011).
[61]J. P. Perdew, K. Burke, and M. Ernzerhof, Phys. Rev. Lett. **77**, 3865 (1996).
[62]P. Haas, F. Tran, P. Blaha, K. Schwarz, and R. Laskowski, Phys. Rev. B **80**, 195109 (2009).
[63]J. P. Perdew, A. Ruzsinszky, G. I. Csonka, O. A. Vydrov, G. E. Scuseria, L. A. Constantin, X. Zhou, and K. Burke, Phys. Rev. Lett. **100**, 136406 (2008).
[64]P. Haas, F. Tran, and P. Blaha, Phys. Rev. B **79**, 085104 (2009).
[65]D. G. Anderson, J. Assoc. Comput. Mach. **12**, 547 (1964).
[66]D. R. Hamann, Phys. Rev. Lett. **42**, 662 (1979).
[67]P. J. Cumpson and M. P. Seah, Surf. Interface Anal. **25**, 430 (1997).
[68]http://lasurface.com/xps/imfpgrapher.php
[69]H. Kobayashi, M. Nagata, R. Kanno, and Y. Kawamoto, Mater. Res. Bull. **29**, 1271 (1994).
[70]J. J. Yeh and I. Lindau, *Atomic Calculation of Photoionization Cross-Sections and Asymmetry Parameters* (Gordon and Breach, Langhorne, PA, 1993).
[71]M. P. Seah and W. A. Dench, Surf. Interface Anal. **1**, 2 (1979).